Check for updates

Biodegradable and Bioabsorbable Polylactic Acid Ferroelectrets with Prominent Piezoelectric Activity

Xingchen Ma, Sergey Zhukov, Heinz von Seggern, Gerhard M. Sessler, Omar Ben Dali, Mario Kupnik, Ying Dai,* Pengfei He, and Xiaoqing Zhang*

Ferroelectrets have promoted a variety of exciting flexible sensors, actuators, and microenergy harvesters. However, most ferroelectrets have been fabricated from non-degradable petro-based resins, and thus the recycling of these materials constitutes a big challenge. This article reports biodegradable and bioabsorbable ferroelectret films made from polylactic acid (PLA) resins for highly sensitive transducer applications, which can operate either in piezoelectric 33 or 31/32 mode. By modification of the microstructure and polarization, pronounced longitudinal and transverse piezoelectric activities are realized in a single material. For samples with a thickness of 400 μm and a bulk density of 350 kg m^{-3}, the Young's moduli in thickness and plane direction are ranging from 0.1 to 10 MPa, respectively. After polarization in the thickness direction, quasi-static piezoelectric d_{33}, g_{33}, d_{31} (d_{32}), and g_{31} (g_{32}) coefficients in the PLA films, up to 500 pC N^{-1}, 40 Vm N^{-1}, −44 pC N^{-1}, and −3.6 Vm N^{-1}, are achieved, respectively. The longitudinal piezoelectric coefficients of the PLA films are comparable to non-degradable polymer ferroelectrets, while the transverse piezoelectric activity is superior, which may be attributed to the reduction of Young's moduli in the plane direction. The preparation procedure of the PLA ferroelectrets is compatible with large-scale production lines and thus can greatly promote their applications in green electronics.

1. Introduction

Since the discovery of strong piezoelectricity in cellular electrets, commonly known as ferroelectrets or piezoelectrets, they have been steadily investigated and widely applied in electromechanical, electroacoustic, and ultrasonic sensors, actuators, and energy harvesters.[1–6] The piezoelectricity in ferroelectrets stems from the electret property of the matrix polymer and the specific cellular structure of the material,[7] which differs significantly from conventional piezoelectric materials.[8,9]

During the last two decades, many efforts have been devoted to developing various ferroelectrets with improved performance, including polypropylene (PP),[10] fluorinated polyethylene propylene (FEP),[6,11] polytetrafluoroethylene (PTFE),[12] polyethylene (PE),[13] polyethylene terephthalate (PETP),[14] polyetherimide (PEI), polyether ether ketone (PEEK),[15] as well as cyclo-olefin polymers (COP)[16] and its copolymers (COC).[17] A variety of superior characteristics, such as large piezoelectric d_{33} coefficients, low acoustic impedance, flexibility, low cost, and easy handling, have been realized in ferroelectrets when compared to conventional piezoelectric materials.[3,18–21] However, a major drawback of such materials has been the poor recycling ability of discarded devices. The reason is that almost all present materials used in ferroelectrets originate from fossil fuels, and the finding of an economic recycling method remains the greatest challenge and may turn out to be harmful to human health. In addition, large transverse piezoelectric activity is desirable for some applications. However, most ferroelectrets so far, with the exception of parallel tunnel FEP ferroelectrets, show very weak transverse piezoelectric response.[4]

X. Ma, X. Zhang
Shanghai Key Laboratory of Special Artificial Microstructure Materials and Technology
School of Physics Science and Engineering
Tongji University
Shanghai 200092, China
E-mail: x.zhang@tongji.edu.cn

The ORCID identification number(s) for the author(s) of this article can be found under https://doi.org/10.1002/aelm.202201070.

S. Zhukov, H. von Seggern
Department of Materials and Earth Sciences
Technical University of Darmstadt
Merckstraße 25, 64283 Darmstadt, Germany

G. M. Sessler, O. Ben Dali, M. Kupnik
Department of Electrical Engineering and Information Technology
Technical University of Darmstadt
Merckstraße 25, 64283 Darmstadt, Germany

Y. Dai, P. He
School of Aerospace Engineering and Applied Mechanics
Tongji University
Shanghai 200092, China
E-mail: ydai@tongji.edu.cn

Thus, ferroelectrets based on biodegradable materials, which have a strong longitudinal piezoelectric response as well as a significant transverse piezoelectric activity, are of great interest.[22]

Polylactic acid (PLA), one of the fastest developing biodegradable materials in recent years, is a kind of biodegradable and bioabsorbable polymer originating from renewable plant sources, such as corn or potato starch, tapioca roots, and sugar canes.[23] After being used, PLA products can be decomposed and degraded into CO_2 and water to re-enter natural circulation. Previous research has demonstrated the electret and piezoelectric properties in PLA-based polymers.[24–26] So far, the first fully biodegradable PLA-based piezoelectric pressure sensor has been developed to control physiological forces.[27]

Our previous work reported the feasibility of fabricating high-performance ferroelectrets with degradable PLA resins by utilizing a preparation procedure that is compatible with an industrial large-scale continuous production line and some preliminary but crucial experimental results.[22] And, detailed information on the biodegradability of the PLA ferroelectrets is disclosed in our very recent publication,[28] showing that such a material has an excellent biodegradability and its degradation can be finished in 11 h as subjected to a hydrothermal degradation process at an elevated temperature of 170 °C. Degradation of the PLA ferroelectrets in natural soil and physiological solution (bioabsorbability) is now being under our long-term research programs. Following the previous work, herein, we systematically investigated the mechanical, electrical, and electromechanical characteristics of such ferroelectrets, and the relation between the longitudinal and transverse piezoelectric effects was explored. It turned out that the fabricated PLA ferroelectrets could not only reproduce the excellent piezoelectric activities of classic ferroelectrets in the longitudinal direction, but also exhibit a significant transverse piezoelectric response in combination with biodegradability and bioabsorbability.

2. Results and Discussion

2.1. Sample Preparation and Microstructure

Since the detailed fabrication process of the ferroelectrets based on PLA polymers has been described in previously published work,[22] only a brief description of this topic is provided here. The raw material adopted for the present study is a modified PLA resin (Guangzhou Bio-plus Materials Technology Co., Ltd., Bio-plus 301H) with a density of 1240 kg m^{-3}. A schematic illustration of the preparation process is shown in **Figure 1**. The preparation starts in our lab with the PLA foam sheets produced in a commercial production line using CO_2 as a foaming agent. The directions $x(1)$, $y(2)$, and $z(3)$ are along the machine direction (MD), perpendicular to the machine direction (CD), and the thickness direction, respectively. A microstructure modification was first carried out on the PLA foam sheets to improve the charging capability and mechanical properties of the materials with a hydraulic press.[29] After that, the modified cellular films were polarized in a tip-to-plane corona setup at room temperature under a negative corona voltage of −25 kV for 5 min to form oriented "macrodipoles" in the thickness direction $z(3)$, as
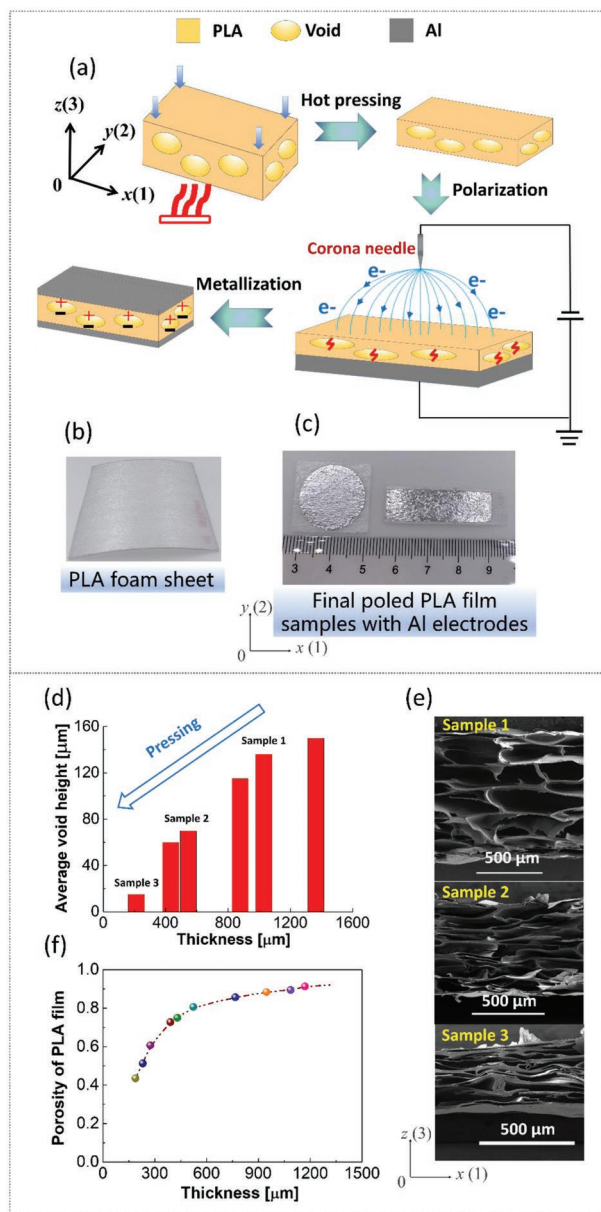

Figure 1. Schematic illustration of the fabrication process of PLA ferroelectrets. a) Specific processes, including hot pressing at an elevated temperature, polarization, and final metallization. b) Photograph of a PLA foam sheet. c) Photographs of the fabricated PLA ferroelectret samples with coated Al electrodes in two geometric shapes. d) Average cell height versus film thickness. e) Cross-sectional SEM images of three PLA films with different thicknesses marked as samples 1, 2, and 3 in Figure 1d. f) Porosity of PLA films versus thickness.

schematically shown in Figure 1a. The trick of the formation of the oriented "macrodipoles" is to charge the cells by subjecting the cellular PLA film to a high electric field, which is generated by the charges deposited on the surface of the film during corona charging. The high electric field generates inside the cells many tiny microplasma discharges similar to lightning, resulting in positive and negative electric charges, which are separated by the corona-induced electric field and therefore deposited on opposite internal cell surfaces.[1,30] Since the

ADVANCED
SCIENCE NEWS
www.advancedsciencenews.com

ADVANCED
ELECTRONIC
MATERIALS
Open Access
www.advelectronicmat.de

polarization is conducted at room temperature, no inversion of inherent dipoles happens. Therefore, the polarized cellular PLA films in this study belong to the category of ferroelectrets, which are different from the conventional piezoelectric PLA materials.

In order to evaluate the electrical performance, 100 nm thick Al electrodes were deposited on both surfaces of the cellular PLA films by physical vapor deposition. Figure 1b,c shows photographs of the foam sheet and two fabricated ferroelectret film samples. Figure 1d presents the average void (or cell) height determined from scanning electron microscopy (SEM) images as a function of the film thickness.

Since PLA foam sheets change their volume when compressed, the cells of the foam collapse as they are pressed in the thickness direction, producing very little lateral spreading once collapse has begun.[31] Therefore, the thickness variation of the PLA foam sheets reflects the deformation of the cells in the direction $z(3)$, and the average height of cells decreases. The plastic deformation of cells of the modified PLA film enhances the anisotropy of the material, leading to the anisotropy of Young's modulus in the directions $x(1)$, $y(2)$, and $z(3)$. The experimental data of the mechanical properties along directions $x(1)$ and $y(2)$, e.g., stress–strain curves (Figure S1, Supporting Information) and in the thickness direction $z(3)$ (Figure S2, Supporting Information), indicate that the extension moduli in directions $x(1)$ and $y(2)$, and the Young's moduli in the thickness direction $z(3)$ are in levels of 10 and 0.1 MPa, respectively. No significant difference in Young's modulus was observed between directions $x(1)$ and $y(2)$ for the presently studied samples, and thus the discussion in the following will only focus on direction $x(1)$.

SEM images of the cross sections of samples marked as 1, 2, and 3, with thicknesses of 1031, 546, and 212 μm, respectively, are presented in Figure 1e. As can be seen, the shapes of the cells undergo a remarkable change in thickness. Since previous study indicates that very flat or very thick cells are undesirable for achieving optimal polarization during corona charging,[25] the thickness of the PLA films in this study was chosen in the range of 150–700 μm. By reducing the thickness from the initial value from 1300 to about 200 μm, the porosity decreased from 90% to 40% (Figure 1f). The porosity of the PLA films was determined by $P_{\text{porosity}} = 1 - \dfrac{\rho_{\text{cellular}}}{\rho_{\text{solid}}}$, where ρ_{solid} and ρ_{cellular} are the densities of the solid PLA polymer of 1240 kg m^{-3} and the cellular PLA film, respectively.[32]

2.2. Longitudinal Piezoelectric Response

The origin of longitudinal piezoelectric response in the PLA ferroelectrets stems from the synergistic effect of the oriented "macrodipoles" formed by separated positive and negative space charges trapped at opposite cell walls and the cellular structure of the film. When a force exerts on the PLA ferroelectret film in thickness direction $z(3)$, the compression occurs mainly in the air-filled cells because of the much softer air compared to the solid PLA polymer matrix, resulting in a reduction of the dipole moment of the "macrodipoles." Therefore, a positive piezoelectric d_{33} coefficient is obtained. It seems that the electromechanical coupling mechanism is different from those of the conventional piezoelectric materials such as lead zirconate titanate (PZT) and ferroelectric polymer polyvinylidene fluoride

(PVDF).[5] The generation of the present piezoelectric effect through the compression of macrodipoles can be predicted with a charge-spring model developed by Gerhard et al.[33]

The longitudinal piezoelectric d_{33} and g_{33} coefficients characterize the piezoelectric response when the external mechanical force F_3 is applied in direction $z(3)$ perpendicular to the surface of the film and along the polarization axis. Let us now consider the quasistatic and dynamic longitudinal piezoelectric responses of the PLA ferroelectrets. First of all, the focus lies on studying the effect of sample thickness on the piezoelectric d_{33} and g_{33} coefficients. To this end, all the samples, polarized under an identical corona voltage of −25 kV for 5 min, were evaporated with Al electrodes on both sides with a size of 20 mm in diameter. In the quasistatic method, a force of $F_3 = 0.98$ N is loaded on the whole electrode area of the sample first, corresponding to an applied pressure of 3.1 kPa, and then rapidly released. The integrated charge Q_3 induced on the electrodes after the force removal is recorded for 10 s with an electrometer (Keithley 6514). During the complete experiment, a static force of 0.25 N, corresponding to a pre-load pressure of 0.8 kPa, is always loaded on the sample to avoid bending effects during force release.[12] A schematic setup is shown in Figure S3a (Supporting Information). The d_{33} and g_{33} coefficients are given by

$$d_{33} = \frac{Q_3}{F_3} \tag{1}$$

$$g_{33} = \frac{d_{33}}{\varepsilon_0 \varepsilon_r} \tag{2}$$

where ε_0 and ε_r are the vacuum permittivity and relative permittivity of the cellular PLA film, respectively. And ε_r can be determined by dielectric spectroscopy.

The piezoelectric d_{33} coefficient as a function of film thickness for the PLA film samples is depicted in **Figure 2**a as a dashed line. As mentioned above, the piezoelectric d_{33} coefficient of the PLA ferroelectret is positive, which is different from that of the ferroelectric polymer PVDF with a negative coefficient.[19] The results indicate that the quasi-static piezoelectric d_{33} coefficient reaches its maximum at 500 pC N^{-1} at a film thickness of about 400 μm. This is a quite high value for the ferroelectrets with an uniform thickness greater than 100 μm.[22] As also noted for other ferroelectrets, the peaked function is generally attributed to the variation of the compressive modulus of the cellular films with thickness. Based on the obtained results of quasi-static compressive Young's modulus Y_3 (inset in Figure 2a; Table S1, Supporting Information) and an typical electrode charge density σ of 0.3 mC m^{-2} (Figure S4, Supporting Information) obtained by contact charging, the theoretical dependence utilizing Equation (3) is plotted as a red solid line in Figure 2a[34]

$$d_{33} = \frac{\sigma}{P} = \frac{\varepsilon_r \cdot t}{Y_3} \frac{t_1 \sum_i t_{2i} \sigma_i}{t_2 (t_1 + \varepsilon_r t_2)^2} = \frac{t_1 \cdot t}{Y_3 \cdot t_2 (t_1 + \varepsilon_r t_2)} \sigma \tag{3}$$

where P denotes the applied pressure (stress); i denotes the total number of air layers; t_1, t_2, and t are the total thicknesses of the solid polymer layers, air gaps, and the cellular film,

ADVANCED
SCIENCE NEWS

www.advancedsciencenews.com

ADVANCED
ELECTRONIC
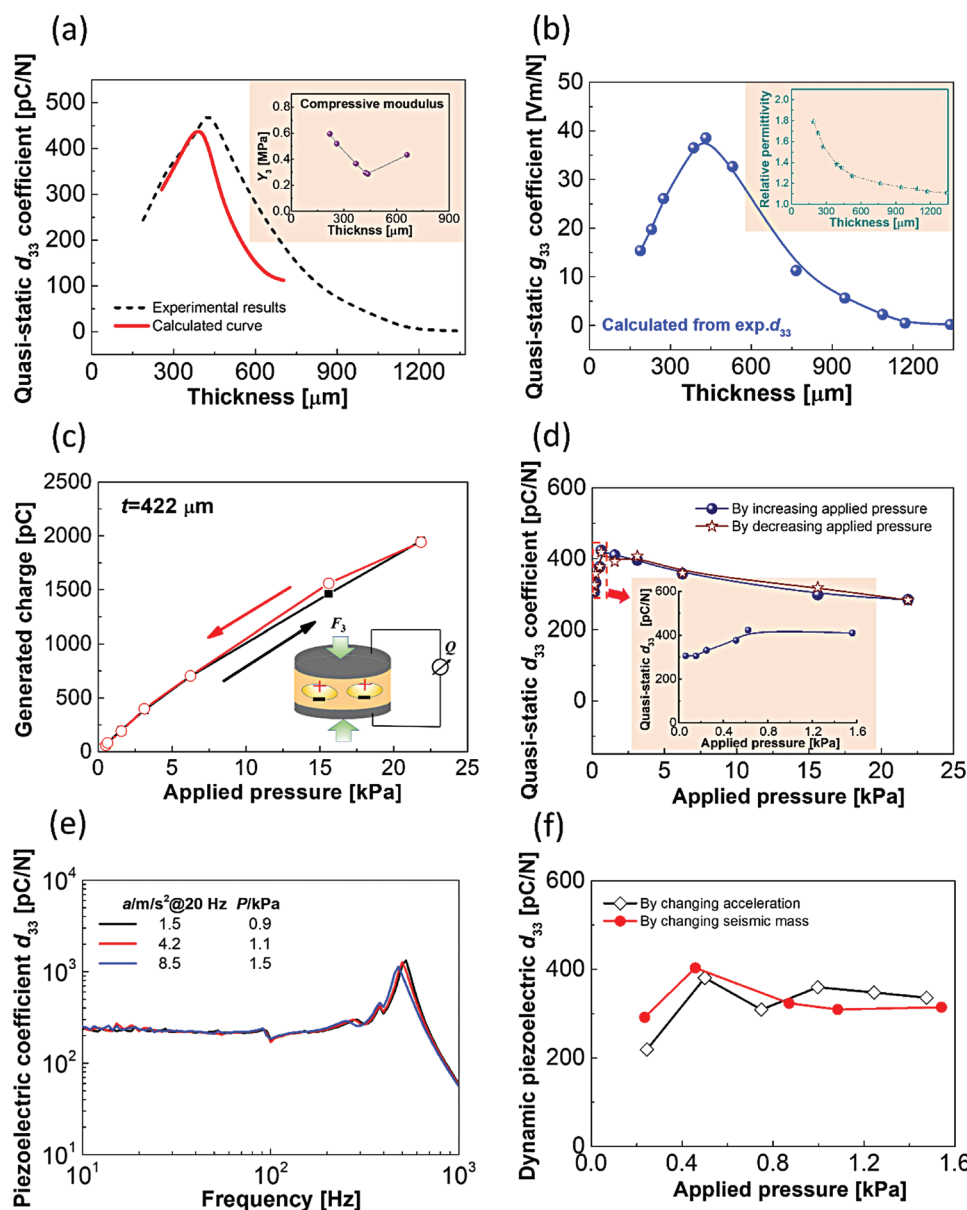**MATERIALS**

www.advelectronicmat.de

Figure 2. Longitudinal piezoelectric response of PLA films. All samples were polarized with a corona voltage of −25 kV for 5 min. a) Measured and calculated quasi-static piezoelectric d_{33} coefficients for PLA samples as a function of thickness. The dashed line represents measured d_{33} coefficients, and the solid line is calculated utilizing Equation (3). Inset shows the dependence of quasi-static compressive Young's modulus Y_3 on thickness. b) Calculated quasi-static piezoelectric g_{33} coefficients for PLA samples as a function of sample thickness. Inset shows the variation of relative permittivity with film thickness. c) Generated charge of PLA ferroelectret sample on the electrodes at different applied pressures. The inset shows the 33-operating mode of the sample. d) Applied pressure dependence of quasi-static piezoelectric d_{33} coefficient for the same sample shown in Figure 2c. Inset indicates the results in the pressure range from 0.06 to 1.6 kPa. e) Frequency dependence of dynamic piezoelectric d_{33} coefficient under various accelerations as indicated. The applied seismic mass is 25 g. f) Dynamic piezoelectric d_{33} coefficient at 100 Hz as a function of applied pressure obtained by either adjusting the acceleration (black open circles) or the seismic masse (solid red dots) for a PLA film sample with a thickness of 176 μm.

respectively; and σ_i refers to the charge density at the interface of air and solid polymer layer. Air thickness t_2 was obtained by multiplying material thickness t with film porosity, while the thickness of the solid polymer layers t_1 was calculated as t minus t_2. The obtained theoretical curve shows a similar shape as the experimental data. The discrepancy between the two curves could be attributed to the larger charge density in the PLA samples polarized by corona charging than the value

used here for the theoretical calculation, which is taken from a contact charged sample. The dependence of the quasistatic d_{33} coefficient on poling voltage for contact charging is shown exemplarily for a 258 μm thickness sample in Figure S5 (Supporting Information). For a poling voltage of −5 kV during contact charging, the d_{33} coefficient is 205 pC N^{-1}, which is smaller than the corresponding value for corona-charged samples with the same thickness, as shown in Figure 2a. Another reason

could be the variation of σ_I for samples with different thicknesses under identical corona charging conditions. The experimental results shown in Figure S4d (Supporting Information) indicate that the "macrodipoles" start to build up at a voltage of 3 kV for the tested sample with a thickness of 350 μm, corresponding to an electric field of 8.5 MV m^{-1}. However, an extensive "macrodipole" has been built up at the same voltage of 3 kV for the sample with a thickness of 258 μm as shown in Figure S5 (Supporting Information), corresponding to an electric field of 11.6 MV m^{-1}. The threshold and optimized polarization electric field and voltages can be predicted with the model developed by Zhukov et al.[35]

Results on the g_{33} coefficients of the PLA samples with various thicknesses are plotted in Figure 2b. The calculated g_{33} coefficients are obtained by utilizing Equation (2) and the corresponding relative permittivity (inset in Figure 2b). The quasistatic g_{33} coefficient reaches its peak value of 40 Vm N^{-1} at a film thickness of about 430 μm.

One of the most important properties of ferroelectrets is the stability of the piezoelectric coefficients under various static and dynamic loads. Therefore, the generated charge of the PLA film samples under a static load ranging from 0 to 22 kPa has been measured exemplarily for the 422 μm thick sample and is displayed in Figure 2c, where the increasing and decreasing pressures are indicated by arrows. The result shows that the samples have good charge stability with very little hysteresis even for relatively high stress values. The correlated quasistatic piezoelectric d_{33} coefficients of the same PLA sample at various applied pressures are plotted in Figure 2d. The results indicate that only marginal differences for the d_{33} coefficients for increasing and decreasing pressures are observed even for different runs. At the same time, it should be noted that with an increase of pressure, the piezoelectric d_{33} coefficient varies between 300 and 420 pC N^{-1}. The inset shows an enlarged view for the sample in a lower pressure range between 0.06 and 1.6 kPa. A stable d_{33} coefficient exists between 0.6 and 1.6 kPa. Similar trends were observed in other PLA ferroelectret samples studied in this research. The variation of d_{33} coefficient with applied pressure can be explained by the nonlinear relation between Young's modulus and applied stress in cellular polymer materials.[36]

In applications such as accelerometers and vibrational energy harvesters, the frequency dependence of the piezoelectric coefficient is of particular importance because these devices normally work in a broad frequency range. Therefore, the dynamic piezoelectric d_{33} coefficient of the PLA ferroelectret films is characterized by using a dynamic shaker as an exciting source. The dynamic piezoelectric d_{33} coefficient is determined as[36]

$$d_{33} = Q_3/ma \tag{4}$$

with m the seismic mass loaded on top of the sample and a the applied dynamic acceleration. The schematic setup can be found in Figure S3b (Supporting Information). Results of the dynamic piezoelectric d_{33} coefficient measured under different acceleration amplitudes are shown in Figure 2e. The utilized PLA sample exhibits an electrode area of 3.14 cm^2 and a thickness of 239 μm. A seismic mass of $m = 25$ g was fixed on the electrode surface of the sample. As shown, a slight decrease of the d_{33} coefficient with increasing frequency up to the resonant frequency at about 479–525 Hz was observed in all cases.[10] The resonance is only weakly damped with increasing acceleration. Above the resonance, the coefficient drops steeply, as expected. The dynamic piezoelectric d_{33} coefficients show a good uniformity with applied pressures between 0.9 and 1.5 kPa, which agrees with the quasi-static results of the identical samples in the same pressure range, as indicated in the inset of Figure 2d. The quasi-static d_{33} coefficient of the tested sample is 539 pC N^{-1} at 3.1 kPa. The dynamic d_{33} coefficient is about 56% of the quasi-static value, known to be mainly attributed to the frequency dependence of Young's modulus Y_3, where the static Y_3 is only 30–50% of the dynamic Y_3 (see Figure S6 in the Supporting Information). Finally, Figure 2f shows the pressure dependence of the dynamic piezoelectric d_{33} coefficients measured at 100 Hz for a PLA sample with a thickness of 176 μm. The black curve was obtained by adjusting the acceleration with a constant seismic mass cemented on the top of the sample, while the red curve was measured at a fixed acceleration by changing the seismic mass. The utilized masses, accelerations, and the applied dynamic forces are shown in Table S2 (Supporting Information). The two curves show good agreement of the dynamic piezoelectric d_{33} coefficient at $\cong 400$ pC N^{-1} for pressures exceeding 0.5 kPa whereby the slight decrease of the piezoelectric coefficients for higher applied pressures is most probably due to the densification of the material, especially the compression of the air voids.[37] The decrease of the dynamic d_{33} coefficient for small pressures could be attributed to the nonlinear stress–strain relation in the cellular PLA films in such a pressure range.

The stability of the piezoelectric d_{33} coefficient in PLA ferroelectrets stored in lab environment ($T = 22 \pm 5$ °C) has been reported in previous work,[22] showing that the decay of the coefficient generally happens in the first 20 days and then becomes stable at about 50% of the initial value, regardless of the thickness of the samples. Additionally, thermally stimulated discharge current (TSDC) spectra in short circuits were measured to further reveal the thermal stability of the charges in the PLA ferroelectret films (Figure S7, Supporting Information). The results indicated that two peaks exist between the temperatures of 50 and 80 °C, meaning that the working temperature of the PLA ferroelectrets is less than 50 °C. For practical applications, disposable devices based on the PLA ferroelectret films may be stored in a freezer before use to keep the sensitivity on a relatively high level.

2.3. Transverse Piezoelectric Responses

Piezoelectric d_{31} and g_{31} coefficients are used to characterize the transverse piezoelectric response of the PLA ferroelectret films. Rectangular film samples with electrodes on both sides were prepared. The electrodes exhibit a length l of 30 mm and a width w of 10 mm. The total width w_0 of the sample is chosen to be slightly larger than the electrode width w to avoid short circuiting around the edges of the electrodes. A static stretching force F_1 along the direction x (1) was applied to the sample with a tensile tester (KJ-1065A). Generated charge Q_3 upon stretching was recorded by an electrometer (Keithley

6514) and the schematic setup is displayed in Figure S8a (Supporting Information). The relationship between the stretching force applied to the active area and the whole sample can be expressed as

$$F_1' = F_1 \cdot \frac{w}{w_0} \qquad (5)$$

where F is the force applied to the whole sample with width of w_0 and F_1' is the force applied to the active (metalized) area with width of w.

The d_{31} and g_{31} coefficients of the PLA ferroelectrets are obtained as follows[4]

$$d_{31} = \frac{Q_3}{F_1'} \cdot \frac{t}{l} \qquad (6)$$

$$g_{31} = d_{31}/\varepsilon_0\varepsilon_r \qquad (7)$$

with t the film thickness and l the length of the metallized sample area. The quasi-static transverse piezoelectric d_{31} coefficients were experimentally determined. Utilizing Equation (7), the related film thicknesses and corresponding permittivity, the g_{31} coefficients were derived and the parameters are summarized in **Table 1**. A quasi-static d_{31} coefficient up to -44 pC N^{-1} for the sample with a thickness of 374 µm, and a g_{31} coefficient of -3.6 Vm N^{-1} for the samples with thicknesses of 374 and 578 µm, respectively, were achieved. The negative piezoelectric d_{31} and g_{31} coefficients in the cellular PLA ferroelectrets are the same as those in the extensively studied ordinary PP ferroelectrets, where the transverse piezoelectric coefficients also have a negative sign.[30]

Dynamic d_{31} coefficients for different stretching forces or stresses were obtained with the setup depicted in Figure S8b (Supporting Information) and are shown in **Figure 3**a. The test sample exhibits an electrode length of 30 mm, a width of 10 mm, and a thickness of 591 µm, respectively. The results obtained with stretching forces of 51 and 167 mN, which are illustrated in black and gray lines, respectively, show little force dependence. Absolute d_{31} values of 8 to 2 pC N^{-1} were measured in the frequency range from 10 to 100 Hz. The drop of the d_{31} coefficient with increasing frequency may be associated with the viscoelastic properties of Poisson's ratio in the material[38] and the enhancement of Young's modulus Y_1 at larger excitation frequencies for cellular polymer films.[36] For larger stretching forces of $\geq$432 mN, corresponding to a stress of
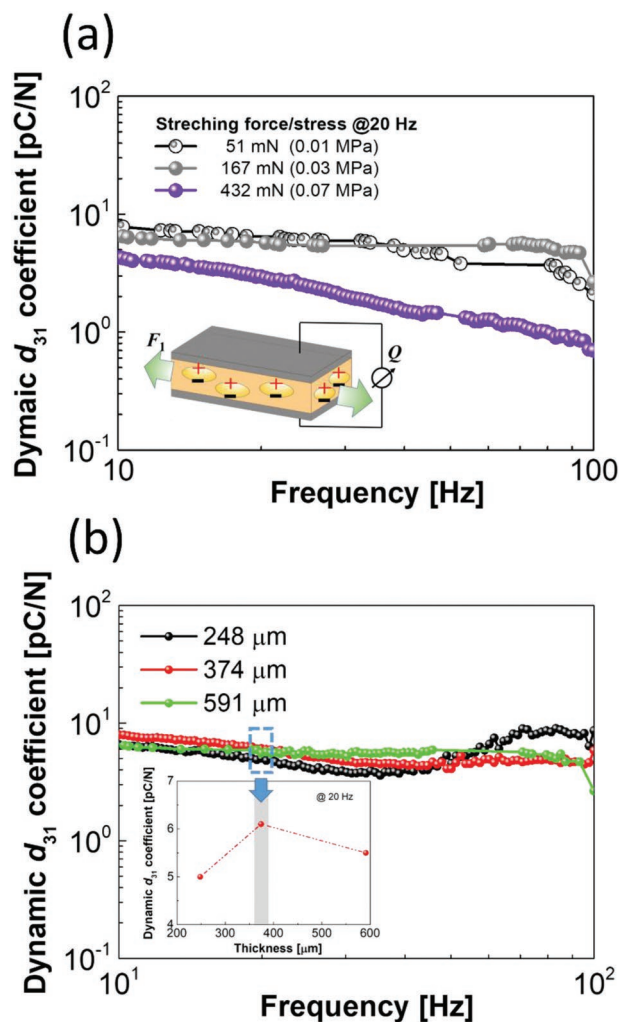

Figure 3. Transverse piezoelectric response of PLA films. a) Frequency dependence of piezoelectric d_{31} coefficient for a PLA sample with a thickness of 591 µm at different stretching stresses. The inset illustrates the schematic of the 31-operating mode. b) Frequency dependence of piezoelectric d_{31} coefficients for PLA samples with different thicknesses. The inset shows the dependence of d_{31} coefficients on film thickness measured at 20 Hz. The d_{31} coefficients have a negative sign but absolute values are shown in this figure.

0.07 MPa, a significant drop of the dynamic d_{31} can be observed over the investigated frequency range, as shown in a purple line in Figure 3a.

Since, however, it is difficult to measure Poisson's ratio of a cellular material, the dependence of the dynamic tension modulus Y_1 on frequency will be determined instead utilizing a dynamic mechanical analyzer (Model DMA 8000). Y_1 for a 360 µm thick PLA sample is shown exemplarily in Figure S9 (Supporting Information). One can see that the dynamic Y_1 increases continuously with frequency from 67 MPa at 0.02 Hz to 90 MPa at100 Hz whereas the quasistatic Y_1 for the cellular PLA sample with the same thickness is only 11 MPa (see **Figure 4**a), indicating that the dynamic value at the smallest measured frequency of 0.02 Hz amounts to 67 MPa, which is 6.1 times larger than the quasi-static value. As indicated in Figure S1 (Supporting Information), samples show two

Table 1. Results of quasi-static d_{31} and g_{31} coefficients for PLA ferroelectrets with various thicknesses. The g_{31} coefficients were calculated utilizing Equation (7) and the experimentally determined d_{31} and the relative permittivity related to the respective film thickness.

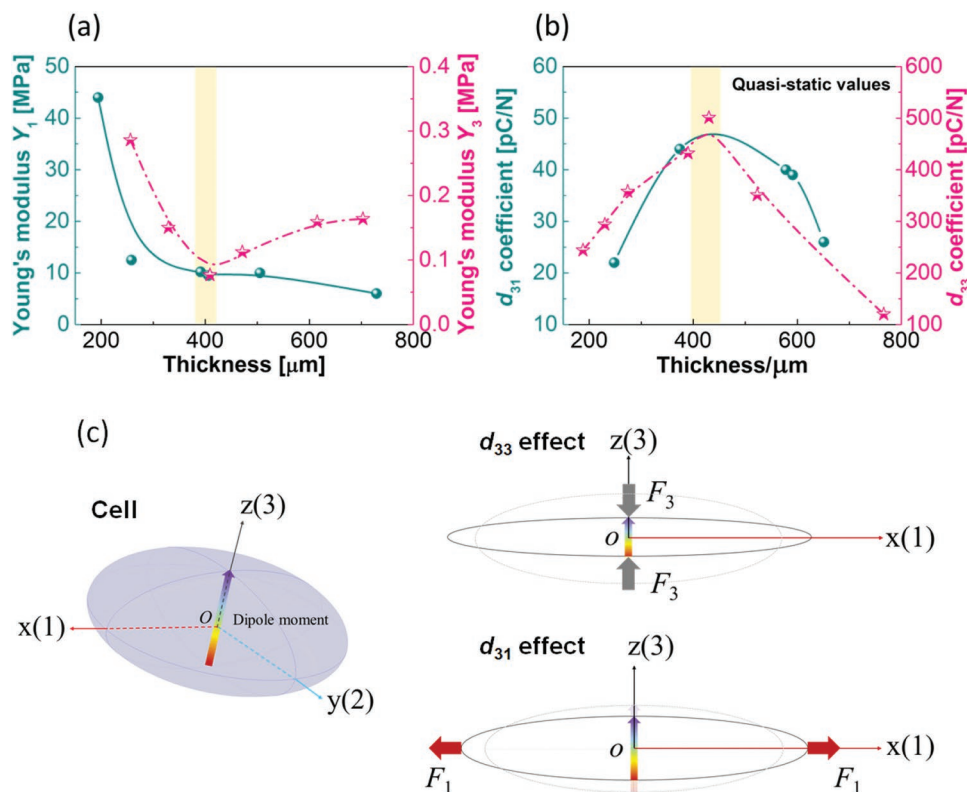| Thickness [µm]	quasi-static d_{31} [pC N^{-1}]	Relative permittivity	quasi-static g_{31} [Vm N^{-1}]
248	−22	1.6	−1.5
374	−44	1.4	−3.6
578	−40	1.3	−3.6
591	−39	1.3	−3.5
651	−26	1.2	−2.4

Figure 4. Dependence of mechanical properties and piezoelectric response on the thickness of PLA ferroelectrets. a) Variation of Young's moduli Y_1 and Y_3 with film thickness. b) Measured quasi-static d_{31} and d_{33} coefficients of PLA ferroelectrets at different film thicknesses. The d_{31} coefficients have a negative sign but absolute values are shown in this figure. c) Schematic diagrams of a flat cell with a dipole moment in the direction $z(3)$ (left) and longitudinal and transverse piezoelectric effects (right).

linear ranges in the stress–stain curve in length direction $x(1)$ if the strain is less than 1.1%. At small strains ranging from 0 to 0.4%, Young's modulus is $\cong$ 10 MPa, about a factor of 2.65 smaller than the corresponding modulus for the strain range of 0.4–1.1%. For the cellular PLA sample of Figure S1 (Supporting Information) with a thickness of $t = 541$ μm, the corresponding stretching force F for the cross section $t \times w$ can be evaluated by $F = \sigma \times t \times w = 216$ mN for a strain of 0.4%. When the stretching force is larger than 216 mN, a larger Young's modulus will cause the drop of the d_{31} coefficient. Figure 3b illustrates the relation between dynamic d_{31} and thickness for three samples utilizing the same stretching force of 167 mN. The samples have been prepared under identical polarization conditions (−25 kV, 2 min). The applied stresses for the samples with thicknesses of 248, 374, and 591 μm are 0.07, 0.04, and 0.03 MPa, respectively. The three samples exhibit similar dynamic d_{31} coefficients over the complete frequency range. At a low frequency of 20 Hz, the sample with the thickness of 374 μm presents the largest d_{31} activity, as indicated in the inset.

2.4. Relationship between Transverse and Longitudinal Piezoelectric Responses

Ferroelectrets are electromechanical coupling materials, and thus both electrical and mechanical properties are involved. For the presently studied cellular PLA films, the polarization is simply directed along the thickness direction $z(3)$. Therefore, to analyze the relationship between transverse and longitudinal piezoelectric responses in the PLA films, mechanical properties in directions $x(1)$ and $z(3)$ are first discussed here. For closed-cell foams, the Young's modulus is strongly dependent on the shape of cells and a sum of three contributions.[31] The first is the contribution of cell-edge (wall) bending. The second contribution is caused by the compression of the cell fluid, which is air in the cellular PLA films and thus can be neglected. And the third contribution is the membrane stress induced by the cell walls.

The quasi-static moduli in directions $x(1)$ and $z(3)$ of the cellular PLA film samples as a function of film thickness are displayed in Figure 4a. The Young's modulus Y_1 was determined for a strain range of 0–0.4% (Figure S1b, Supporting Information) and decreases with increasing of film thickness. A sharp decrease is observed for increasing sample thickness from 200 to 300 μm (Figure 4a), where the elastic response is dominated by cell-wall stretching.[39] The slight decrease of Y_1 with increasing film thickness ranging from 300 to 720 μm from 10 to 5 MPa is probably associated with the shape of cells,[31] where a better understanding of the involved components contributing to Y_1 needs more future research. It has to be mentioned that for PLA films with a thickness larger than 300 μm, the extension moduli are much smaller than those of ordinary PP ferroelectrets.[40] Since, however, smaller extension moduli in the length direction of the films are supporting large transverse

d_{31} piezoelectric coefficients, this result is of great interest for the present study.

The dependence of the compressive Young's modulus Y_3 on the film thickness is shown also in Figure 4a, where Y_3 ranges from 0.1 to 0.3 MPa, two orders of magnitude smaller than Y_1. The related applied force F_3 ranging from 5 to 10 N is shown together with more detailed experimental data in Table S1 (Supporting Information). It should be noted that a V-shaped dependence of Y_3 seems to be a typical characteristic of ferroelectret films containing flat cells.[7] With this knowledge, it can be concluded that the low Young's modulus Y_3 of the cellular PLA films is related to the cellular structure with flat cells where bending of the cell wall under compression may reduce the modulus. This may be reasonably explained by the bending and buckling of the flat part of the cell under force F_3. In addition, it has been reported that anisotropic foams with flat lens-like air cells with an aspect ratio of length to height greater than 4 usually exhibit rather low compressive moduli.[41,42] For the present study, PLA film samples with a thickness of about 400 μm have an aspect ratio of ≈7.7. The minimum value of about 0.1 MPa was obtained in a film sample with a thickness of 400 μm corresponding to the Young's modulus of enclosed air under the pressure of 1 atm. It should be pointed out that a decrease of the film thickness down to 250 μm densifies the material (Figure 1e), resulting in a significant enhancement of Y_3 to 0.3 MPa, and an increase in film thickness to 700 μm also leads to an increase of Y_3 to 0.15 MPa (both shown in Figure 4a). The latter increase could be due to a slight upward orientation of the side walls with increasing cell or wall thickness both increasing the necessary stress for wall bending.

Figure 4b presents the dependence of the measured quasi-static d_{31} and d_{33} coefficients as a function of thickness for the PLA ferroelectrets. The d_{33} coefficients exhibit the expected inverse curvature as Y_3, and the maximal d_{33} coefficient agrees with the minimum of Y_3, at ≈400 μm. For the d_{31} coefficient, the maximum value is also obtained at the film with a thickness close to 400 μm. Poisson's ratio, defined as the negative ratio of the lateral to the axial strain,[43] links the piezoelectric coefficients d_{33} and d_{31} (because the lateral expansion is force free). The Poisson ratio η_{13} is defined as[43]

$$\eta_{13} = \frac{-\varepsilon_3}{\varepsilon_1} \tag{8}$$

where ε_1 and ε_3 are the uniaxial strain and the lateral strain, respectively. For cellular PLA films, Poisson's ratio depends on the details of the cell shape but not on the relative density,[31] and is time dependent.[38] Therefore, the deformation in the thickness $z(3)$ direction induced by the extension in the $x(1)$ direction results in the transverse piezoelectric d_{31} effect. When the extracting force F_1 is applied along the direction $x(1)$, the uniaxial extension is accompanied by a contraction in the transverse direction $y(2)$ and a contraction in the $z(3)$ direction. Because of the complexity of the microstructure and cell shapes in the cellular PLA films, as shown in Figure 1e, and the difficulty of measuring Poisson's ratios directly, the origin of the large transverse piezoelectric activity can only schematically be shown in Figure 4c and explained qualitatively. Since the films are polarized in the direction $z(3)$, the dipole moment in all cells is aligned in the same direction as shown

in Figure 4c. The amount of trapped charge (polarization) can be measured (Figure S4d, Supporting Information) and depends on the applied voltage, the film thickness, the void structure of the film, and the resulting field strength in the individual stacked voids. Since these stacked voids are different in width and length, and surrounded by differently thick walls, it turns out to be very difficult to predict the trapped polarization exactly as has been investigated for geometrically simpler cell structures, like a single-wall tube. Such a study has been carried out allowing us to determine the remnant charge density for an applied corona voltage V_C.[35] The crucial parameter connecting the two piezoelectric effects is Poisson's ratio for the two directions. Therefore, it is necessary to quantitatively investigate the relationship between the longitudinal and transverse piezoelectric effects in case of less complex structures, since it postulates the key influence factors. Relevant study is on the way, and results will be published in future work.

Table 2 compares the Young's moduli, charge density, and piezoelectric coefficients of some piezoelectric materials. Comparisons are made with one type of conventional biodegradable piezoelectric material[27,44,45] and two ferroelectrets with uniform thickness.[29,40,46] Although the piezoelectric mechanism in the PLA ferroelectrets discussed in the present work is different from that in the conventional piezoelectric materials as discussed above, they can all be classified as piezoelectric active materials with the same mechanical–electrical coupling effect. The values clearly indicate that the biodegradable and bioabsorbable cellular PLA films show a highly comparative performance with other piezoelectric materials. By adjusting the mechanical properties of cellular films through commonly used hot pressing processes, prominent multi-dimensional piezoelectric responses can be obtained, providing new opportunities for future biomaterial-based sensors, actuators, and energy harvesters. In particular, the longitudinal quasi-static piezoelectric d_{33} response of the 400 μm thick PLA film surpasses other polymer systems presented in Table 2. It should be noted that d_{33} and d_{31} are not the only factors for evaluating energy harvesting performance, and for piezoelectric materials, the energy harvesting figure of merit (FoM) is expressed as[4]

$$\text{FOM}_{33} = d_{33} \times g_{33} = \frac{d_{33}^2}{\varepsilon_0 \varepsilon_r} \text{ and } \text{FOM}_{31} = d_{31} \times g_{31} = \frac{d_{31}^2}{\varepsilon_0 \varepsilon_r} \tag{9}$$

As can be clearly seen from Table 2, the advantage of PLA ferroelectrets over other piezoelectric materials lies in the combination of the low moduli and high piezoelectric charge/voltage coefficients, which makes these systems especially attractive for sensing and energy harvesting applications.

3. Conclusion

In conclusion, novel ferroelectrets featured with biodegradability and bioabsorbability were made from PLA resins by using a preparation procedure, which is compatible with industrial large-scale production lines.[22] A series of cellular PLA ferroelectret films with thickness ranging from 150 to 700 μm were successfully prepared. For the PLA ferroelectret with a thickness of about 400 μm, the Young's modulus in the thickness

**ADVANCED
SCIENCE NEWS**

www.advancedsciencenews.com

**ADVANCED
ELECTRONIC
MATERIALS**

www.advelectronicmat.de

Table 2. Young's moduli, charge density, and piezoelectric coefficients of some materials. Comparisons are made with one type of conventional biodegradable piezoelectric materials (poly($_L$-lactic acid) (PLLA)), two ferroelectrets with uniform thickness (polypropylene (PP) and irradiation-crosslinked polypropylene (IXPP)).

Materials [Reference]	Y_1 [MPa]	Y_2 [MPa]	Y_3 [MPa]	Charge density [mC m^{-2}]	Relative permittivity	d_{33} [pC N^{-1}]	g_{33} [Vm N^{-1}]	d_{31} [pC N^{-1}]	g_{31} [Vm N^{-1}]	d_{14} [pC N^{-1}]
PLLA[44]	3200	3200	3200	–	4.05	–	–	–	–	≈10
PLLA[27]	5000	5000	5000	–	–	–	–	–	–	≈11
PLLA[45]	25.4	25.4	20	–	–	–	–	–	–	19
PP[40]	10^3	10^3	1	0.5	1.2	140	13	−2	−0.2	–
IXPP[29,46]	6.3	–	0.7	–	1.6	400	28	–	–	–
PLA (This work)	10	16	0.1	0.3	1.4	500	40	−44	−3.6	–

direction and the extension modulus in the length direction are in the levels of 10 and 0.1 MPa, respectively, and the quasi-static piezoelectric d_{33}, g_{33}, d_{31}, and g_{31}, up to 500 pC N^{-1}, 40 Vm N^{-1}, −44 pC N^{-1}, and −3.6 Vm N^{-1}, respectively, were achieved. The longitudinal piezoelectric activity of the PLA ferroelectret films is comparable to that of the ferroelectrets reported in literature but companied with a larger thickness, which is favorable for some applications such as microphones. The quasi-static transverse piezoelectric coefficient of the PLA films is one order of magnitude larger than that of most reported ferroelectrets. Thus, due to the superiority of such PLA ferroelectrets, they are very promising candidates in all kinds of green electronics, such as disposable biosensors/bioactuators and micro-energy-harvesters.

4. Experimental Section

In actual experimental characterization, several samples were adopted in each experiment in this study but only typical results were presented in the article.

Longitudinal Piezoelectric Response Characterization: The longitudinal piezoelectric d_{33} and g_{33} coefficients were used to characterize the piezoelectric response when the mechanical force F_3 was applied in the $z(3)$ direction perpendicular to the surface of the film.[36] Circular samples with an electrode diameter of 20 mm were adopted. In the quasi-static method, a force of $F_3 = 0.98$ N (3.1 kPa) was applied on the sample first, and then it was rapidly removed. The integrated induced electrode charge Q_3 in short circuit after force removal for up to 10 s was recorded through an electrometer (Keithley 6514). During measurement, a preload of 0.25 N was placed on the sample continuously to avoid bending effects of the samples.[12] The d_{33} coefficient is given by $d_{33} = \frac{Q_3}{F_3}$. According to the relationship between d and g coefficients, g_{33} can be obtained by $g_{33} = d_{33}/\varepsilon_0\varepsilon_r$, where ε_0 and ε_r are the permittivity of vacuum and relative permittivity of the PLA film.

In the dynamic method, a cylindrical weight with a seismic mass of m was pasted on top of the PLA sample through adhesive tape. The whole device was then placed on an electrodynamic shaker (B&K 4809). The sinusoidal signal in a wide frequency range (from 10 to 1000 Hz) was fed to the shaker by an audio analyzer (Digital Audio Analyzer, dScope Series III) through a power amplifier (B&K 2713). In response to the excitation signal, the PLA sample was periodically triggered by the seismic mass in the thickness direction. The charge Q_3 generated by the sample in short circuit flew through a charge amplifier (B&K Charge Amplifier Type 2635) and then was measured in real time using an audio analyzer. An accelerometer (B&K 4393), which was first assembled on the shaker and then connected to the audio analyzer through a Conditioning Amplifier (B&K 2692), was used to obtain the dynamic force F_3. The dynamic

piezoelectric d_{33} coefficient was determined by $d_{33} = \frac{Q_3}{F_3} = \frac{Q_3}{ma}$,[36] where a denotes the applied acceleration. Measurement setup for quasi-static and dynamic d_{33} coefficients in PLA ferroelectret films can be found in Figure S3 (Supporting Information).

Transverse Piezoelectric Response Characterization: For determining transverse piezoelectric d_{31} and g_{31} coefficients, rectangular PLA samples with an electrode length l of 30 mm and a width w of 10 mm were used. The total width w_0 of the sample was designed to be slightly larger than the electrode width w in order to avoid potential short circuit around the edges of the electrodes. A static force F_1 was applied to the transverse $x(1)$ direction of the sample with a tensile tester (KJ-1065A). Generated charge Q_3 upon stretching was recorded through an electrometer (Keithley 6514) and the schematic setup is displayed in Figure S8a (Supporting Information). The relationship between the stretching forces applied to the active part and the whole sample is given by $F_1' = F_1 \cdot \frac{w}{w_0}$, where F_1 is the stretching force applied to the whole sample. The d_{31} and g_{31} coefficients of the PLA ferroelectrets were obtained by $d_{31} = \frac{Q_3}{F_1'} \cdot \frac{t}{l}$ and $g_{31} = d_{31}/\varepsilon_0\varepsilon_r$, respectively.[36]

In the dynamic method, two terminals of the strip sample pointing in the $x(1)$ direction were clamped tightly for stretched force application. A force transducer was employed to measure the sinusoidal stretching force generated by the shaker (B&K 4809) which was triggered by controlled signals generated by an audio analyzer (Digital Audio Analyzer, dScope Series III) and amplified by a power amplifier (B&K 2713). The signal of the force sensor was recorded by the audio analyzer with a conditioning amplifier (B&K 2692). Upon excited vibration, the PLA sample sustained a cyclic stretching in the length direction. The generated charge Q_3 in short circuit flew into a charge amplifier (B&K Charge Amplifier Type 2635) and then was recorded by the audio analyzer. Measurement setup for quasi-static and dynamic d_{31} coefficients in PLA ferroelectret films can be found in Figure S8 (Supporting Information).

Supporting Information

Supporting Information is available from the Wiley Online Library or from the author.

Conflict of Interest

The authors declare no conflict of interest.

Data Availability Statement

The data that support the findings of this study are available from the corresponding author upon reasonable request.

Keywords

bioabsorbable, biodegradable, ferroelectret, longitudinal and transverse piezoelectric effect, polylactic acid

[1] S. Bauer, R. Gerhard-Multhaupt, G. M. Sessler, *Phys. Today* **2004**, *57*, 37.

[2] I. M. Graz, M. Kaltenbrunner, C. Keplinger, R. Schwodiauer, S. Bauer, S. Lacour, S. Wagner, *Appl. Phys. Lett.* **2006**, *89*, 073501.

[3] B. Wang, C. Liu, Y. Xiao, J. Zhong, W. Li, Y. Cheng, B. Hu, L. Huang, J. Zhou, *Nano Energy* **2017**, *32*, 42.

[4] X. Zhang, P. Pondrom, G. M. Sessler, X. Ma, *Nano Energy* **2018**, *50*, 52.

[5] X. Mo, H. Zhou, W. Li, Z. Xu, J. Duan, L. Huang, B. Hu, J. Zhou, *Nano Energy* **2019**, *65*, 104033.

[6] S. Zhukov, H. von Seggern, X. Zhang, Y. Xue, O. Ben Dali, P. Pondrom, G. M. Sessler, M. Kupnik, *Adv. Eng. Mater.* **2020**, *22*, 1901399.

[7] A. Mohebbi, F. Mighri, A. Ajji, D. Rodrigue, *Adv. Polym. Technol.* **2018**, *37*, 468.

[8] Z. Butt, R. A. Pasha, F. Qayyum, Z. Anjum, N. Ahmad, H. Elahi, *J. Mech. Sci. Technol.* **2016**, *30*, 3553.

[9] H. Ohigashi, *J. Appl. Phys.* **1976**, *47*, 949.

[10] X. Zhang, J. Hillenbrand, G. M. Sessler, *Appl. Phys. Lett.* **2004**, *85*, 1226.

[11] S. Zhukov, D. Eder-Goy, C. Biethan, S. Fedosov, B.-X. Xu, H. von Seggern, *Smart Mater. Struct.* **2018**, *27*, 015010.

[12] X. Zhang, X. Zhang, G. M. Sessler, X. Gong, *J. Phys. D: Appl. Phys.* **2014**, *47*, 015501.

[13] O. Hamdi, F. Mighri, D. Rodrigue, *J. Appl. Polym. Sci.* **2019**, *136*, 47646.

[14] M. Wegener, W. Wirges, R. Gerhard-Multhaupt, *Adv. Eng. Mater.* **2005**, *7*, 1128.

[15] N. Behrendt, C. Greiner, F. Fischer, T. Frese, V. Altstadt, H.-W. Schmidt, R. Giesa, J. Hillenbrand, G. M. Sessler, *Appl. Phys. A* **2006**, *85*, 87.

[16] E. Saarimaki, M. Paajanen, A.-M. Savijarvi, H. Minkkinen, M. Wegener, O. Voronina, R. Schulze, W. Wirges, R. Gerhard-Multhaupt, *IEEE Trans. Dielectr. Electr. Insul.* **2005**, *13*, 963.

[17] G. C. Montanari, D. Fabiani, F. Ciani, A. Motori, M. Paajanen, R. Gerhard-Multhaupt, M. Wegener, *IEEE Trans. Dielectr. Electr. Insul.* **2007**, *14*, 238.

[18] Y. M. Yousry, K. Yao, S. Chen, W. H. Liew, S. Ramakrishna, *Adv. Electron. Mater.* **2018**, *4*, 1700562.

[19] J. Yang, Q. Chen, F. Xu, H. Jiang, W. Liu, X. Zhang, Z. Jiang, G. Zhu, *Adv. Electron. Mater.* **2020**, *6*, 10.

[20] C. S. Han, A. Cho, D. B. Kim, Y. S. Cho, *Adv. Electron. Mater.* **2018**, *4*, 7.

[21] W. Gao, L. You, Y. Wang, G. Yuan, Y. Chu, Z. Liu, J. Liu, *Adv. Electron. Mater.* **2017**, *3*, 1600542.

[22] S. Zhukov, X. Ma, H. von Seggern, G. M. Sessler, O. Ben Dali, M. Kupnik, X. Zhang, *Appl. Phys. Lett.* **2020**, *117*, 112901.

[23] E. Castro-Aguirre, F. Iniguez-Franco, H. Samsudin, X. Fang, R. Auras, *Adv. Drug Delivery Rev.* **2016**, *107*, 333.

[24] E. Galikhanov, I. Lounev, A. Guzhova, Y. Gusev, M. Galikhanov, M. Vasilyeva, *AIP Conf. Proc.* **2016**, *1722*, 290002.

[25] X. Gao, L. Huang, B. Wang, D. Xu, J. Zhong, Z. Hu, L. Zhang, J. Zhou, *ACS Appl. Mater. Interfaces* **2016**, *8*, 35587.

[26] J. Morvan, E. Buyuktanir, J. L. West, A. Jákli, *Appl. Phys. Lett.* **2012**, *100*, 063901.

[27] E. J. Curry, K. Ke, M. T. Chorsi, K. S. Wrobel, A. N. Miller, A. Patel, I. Kim, J. Feng, L. Yue, Q. Wu, C. Kuo, K. W.-H. Lo, C. T. Laurencin, H. Ilies, P. K. Purohit, T. D. Nguyen, *Proc. Natl. Acad. Sci. USA* **2018**, *115*, 909.

[28] X. Ma, Q. Hu, Y. Dai, P. He, X. Zhang, *Sens. Actuators, A* **2022**, *346*, 113834.

[29] X. Zhang, L. Wu, G. M. Sessler, *AIP Adv.* **2015**, *5*, 7.

[30] M. Lindner, H. Hoislbauer, R. Schwodiauer, S. Bauer-Gogonea, S. Bauer, *IEEE Trans. Dielectr. Electr. Insul.* **2004**, *11*, 255.

[31] L. J. Gibson, M. F. Ashby, *Cellular Solid: Structure and Properties*, Cambridge University Press, Cambridge **1999**.

[32] P. Fang, X. Ma, X. Li, X. Qiu, R. Gerhard, X. Zhang, G. Li, *IEEE Sens. J.* **2018**, *18*, 1.

[33] R. Gerhard, S. Bauer, X. Qiu, in 2016 IEEE Conf. on Electrical Insulation and Dielectric Phenomena (CEIDP), IEEE, Canada, NJ **2016**, p. 81.

[34] G. M. Sessler, J. Hillenbrand, *Appl. Phys. Lett.* **1999**, *75*, 3405.

[35] S. Zhukov, D. Eder-Goy, S. Fedosov, B. X. Xu, H. von Seggern, *Sci. Rep.* **2018**, *8*, 4597.

[36] X. Ma, H. von Seggern, G. M. Sessler, S. Zhukov, O. Ben Dali, M. Kupnik, X. Zhang, *Smart Mater. Struct.* **2020**, *30*, 015002.

[37] X. Zhang, J. Huang, J. Chen, Z. Wan, S. Wang, Z. Xia, *Appl. Phys. Lett.* **2007**, *91*, 182901.

[38] N. W. Tschoegl, W. G. Knauss, I. Emri, *Mech. Time-Depend. Mater.* **2002**, *6*, 3.

[39] S. Malek, L. Gibson, *Mech. Mater.* **2015**, *91*, 226.

[40] G. S. Neugschwandtner, R. Schwödiauer, M. Vieytes, S. Bauer-Gogonea, S. Bauer, J. Hillenbrand, R. Kressmann, G. M. Sessler, M. Paajanen, J. Lekkala, *Appl. Phys. Lett.* **2000**, *77*, 3827.

[41] M. Wegener, S. Bauer, *ChemPhysChem* **2005**, *6*, 1014.

[42] Y. Zhang, C. R. Bowen, S. K. Ghosh, D. Mandal, H. Khanbareh, M. Arafa, C. Wan, *Nano Energy* **2019**, *57*, 118.

[43] A. C. Eringen, *J. Appl. Mech.* **1962**, *31*, 368.

[44] C. Zhao, J. Zhang, Z. L. Wang, K. Ren, *Adv. Sustainable Syst.* **2017**, *1*, 1700068.

[45] E. J. Curry, T. T. Le, R. Das, K. Ke, E. M. Santorella, D. Paul, M. T. Chorsi, K. T. M. Tran, J. Baroody, E. R. Borges, B. Ko, A. Golabchi, D. Xin, D. Rowe, L. Yue, J. Feng, M. D. Morales-Acosta, Q. Wu, I. P. Chen, X. T. Cui, J. Pachter, T. D. Nguyen, *Proc. Natl. Acad. Sci. USA* **2020**, *117*, 214.

[46] X. Zhang, X.-W. Zhang, Q. You, G. M. Sessler, *Macromol. Mater. Eng.* **2014**, *299*, 3.